# Nanoscale

## PAPER

# Networks of as-dispersed, polymer-wrapped (6,5) single-walled carbon nanotubes for selective Cu²⁺ and glyphosate sensing†

Merve Balcı Leinen, Sebastian Lindenthal, Daniel Heimfarth and Jana Zaumseil [ID] *

Networks of semiconducting single-walled carbon nanotubes (SWNTs) can be used as the transducing layer for sensors based on water-gated transistors. To add specific sensing capabilities, SWNTs are often functionalized with additional moieties or selective membranes are applied, thus increasing the complexity of the fabrication process. Here we demonstrate that drop-cast networks of monochiral (6,5) SWNTs, which are commonly dispersed in organic solvents with the polyfluorene–bipyridine copolymer PFO-BPy, can be employed directly and without additional functionalization or ion-selective membranes to detect Cu²⁺ ions over a wide range of concentrations in aqueous solutions. The observed voltage shifts of water-gated transistors with these (6,5) SWNT networks directly correlate with the cupric ion concentration. They result from induced n-doping due to the complexation of positive copper ions to the bipyridine units of the wrapping polymer. Furthermore, the competitive binding of Cu²⁺ to the herbicide glyphosate as well as to biologically relevant pyrophosphates can be used for the direct detection and quantification of these molecules at nano- to micromolar concentrations.

## Introduction

Dispersions of purely semiconducting single-walled carbon nanotubes (SWNTs) are suitable inks for the creation of active thin films in a wide range of (opto-)electronic devices – especially field-effect transistors – using various solution processing techniques such as ink-jet printing,[1,2] aerosol jet printing[3–6] or even just spin-coating[7] or dip-coating.[8] Excellent semiconducting purities above 99.9% are attainable with modern separation and selective dispersion techniques.[9] They ensure high charge carrier mobilities combined with high on/off current ratios and large scale reproducibility.[10] One application of solution-processed random networks of SWNTs that benefits strongly from these advances is sensors. Both chemiresistive sensors[11] and those based on electrolyte-gated field-effect transistors[12–14] show much higher responsivities and selectivities when fabricated with purely semiconducting and ideally monochiral nanotubes instead of mixed networks.[15] The high charge carrier mobilities, mechanical flexibility and large surface area of SWNT networks in combination with their chemical stability make them a highly suitable and versa-

tile transducer material for sensors compared to, *e.g.*, organic semiconductors. Furthermore, selectivity toward a certain analyte can be achieved through covalent or non-covalent functionalization of SWNTs with *e.g.*, DNA,[16,17] nano-bodies,[18] enzymes,[19] or various other stimuli-responsive functional groups.[20–23] Here we investigate sensors based on water-gated field-effect transistors that use random SWNT networks as the semiconducting material. For the detection of metal ions with such transistors (*e.g.*, for sweat analysis[24]) ion-selective membranes with specific ionophores have been widely used, *e.g.*, for Na⁺,[25] K⁺ and Ca²⁺.[26] The sensor response to increasing concentrations of the corresponding ions is typically a shift of the threshold or turn-on voltage. Ion-selective membranes offer high selectivity and versatility but also require additional processing steps and thus increase device complexity and cost.

In the above types of sensors the SWNT network itself is seen as largely neutral with respect to the analyte.[13] However, the dispersion of SWNTs and formulation of inks already requires specific surfactants or polymers that may also interact with certain analytes. In particular, the selective dispersion of semiconducting carbon nanotubes in organic solvents relies on conjugated polymers often containing functional moieties along their backbone (*e.g.*, pyridines, carbazoles, thiophenes)[27–29] or sidechains,[23,30] which may intentionally or unintentionally interact with ions or gas molecules. The most commonly used polymers for the selective dispersion of nanotubes are polyfluorenes[31] and polycarbazoles.[32] The highest

*Institute for Physical Chemistry, Universität Heidelberg, D-69120 Heidelberg, Germany. E-mail: zaumseil@uni-heidelberg.de*

†Electronic supplementary information (ESI) available: Spectroscopic characterisation of dispersions, conditioning of devices with different nanotube networks, pyrophosphate sensing. See DOI: https://doi.org/10.1039/d2nr02517e

selectivity for a single nanotube species – the (6,5) SWNTs – has been demonstrated with the polyfluorene–bipyridine copolymer PFO-BPy,[33] which can be applied on a large scale[34] and has also been used for the dispersion of large diameter semiconducting nanotubes for devices,[35] including sensors.[13]

Here, we demonstrate that drop-cast networks of PFO-BPy wrapped (6,5) SWNTs can be used directly and without any additional functionalization in water-gated transistors to selectively detect $Cu^{2+}$ ions over a wide range of concentrations. Furthermore, the competitive binding of $Cu^{2+}$ to the herbicide glyphosate as well as pyrophosphate is used for their direct detection and quantification at low concentrations.

## Results and discussion

The polyfluorene-based wrapping-polymers poly[(9,9-dioctylfluorenyl-2,7-diyl)-*alt*-(6,6'-[2,2'-bipyridine])] (PFO-BPy) and poly(9,9-dioctylfluorene) (PFO) were employed to selectively disperse semiconducting SWNTs in toluene from CoMoCat raw material as depicted in Fig. 1a. After removal of unbound polymer, drop-cast networks of SWNTs were applied as the active transducing layers in water-gated transistors and investigated in terms of their sensing capabilities toward various metal ions. The copolymer PFO-BPy wraps almost exclusively (6,5) SWNTs, while PFO yields a mixture of nanotubes consisting predominantly of (7,5) SWNTs and small amounts of (6,5) and (7,6) SWNTs (see also ESI, Fig. S1†). The two majority nanotube species have slightly different but still comparable bandgaps (1.27 eV and 1.21 eV)[36] and should behave very similarly as semiconducting layers (*i.e.*, similar carrier mobilities and injection barriers). The main difference between the two wrapping polymers is the presence of the bipyridine unit in PFO-BPy, which was previously shown to enable complexation with $Re(CO)_5Cl$ and unwrapping of the polymer from the SWNTs in dispersion.[37,38]

As illustrated in Fig. 1b, the transistors with polymer-wrapped SWNT networks were operated by water-gating. A custom-made PTFE reservoir was employed to enclose the interdigitated source/drain electrodes (channel length 20 μm, channel width of 10 mm) and a large side-gate (all Cr/Au). The reservoir was filled with de-ionized (DI) water or the aqueous solutions of the corresponding analytes as the electrolyte. Note that due to the autoprotolysis of water there is always a sufficient concentration of ions available for gating even without additional electrolytes.[39]

Prior to the acquisition of the presented transfer characteristics, all devices were conditioned by collecting ten consecutive cycles of transfer curves to ensure equilibration. The conditioning cycles of a transistor with a PFO-BPy wrapped SWNT network are shown in Fig. S2 (ESI†) including those for the corresponding analytes. They confirm that in all cases a stable state was reached already after the second cycle and no additional shifts occurred after that. All water-gated transistors showed only hole-transport within the investigated gate voltage range, as expected for large-bandgap SWNTs contacted by gold electrodes in water. The gate currents (leakage) were always at least one order of magnitude below the drain on-currents. Current hysteresis remained small. Only forward sweeps are shown and used in the following to extract voltage shifts.

After conditioning, transfer characteristics were acquired at low drain voltages ($V_d$ = −0.1 V) by sweeping the gate voltage ($V_g$) between 0.8 V and −0.8 V as shown in Fig. 2a for a transistor with a PFO-BPy-wrapped SWNT network (PFO-BPy/CoMoCat). First, transfer curves were collected for pure water and recorded as the blank and reference for the cation analyte measurements. Next, aqueous solutions of $Zn^{2+}$, $Ni^{2+}$, $Cr^{3+}$, $Fe^{3+}$, $Ag^+$ and finally $Cu^{2+}$ (all with nitrate anions) at a metal ion concentration of 15 μM were introduced in the given order and the corresponding transfer curves were collected following the standardized conditioning steps (see Fig. S2, ESI†). After the removal of each analyte solution, another cycle of conditioning steps was performed with fresh DI water to ensure the consistency of the blank measurements before introducing the next analyte. A selection of transfer characteristics (only forward sweeps) is shown in Fig. 2a where a clear turn-on voltage shift to more negative values can be observed in the presence of $Cu^{2+}$ ions accompanied by a slight increase in the
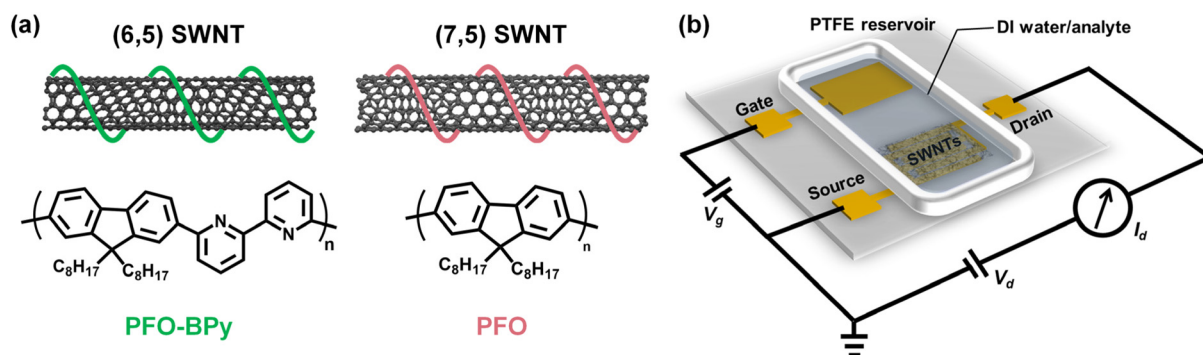


**Fig. 1** (a) Molecular structures of PFO–BPy and PFO as wrapping polymers for (6,5) and (7,5) nanotubes, respectively. (b) Schematic illustration of a water-gated field-effect transistor with a large side-gate and a polymer-wrapped SWNT network drop-cast on interdigitated source/drain electrodes.
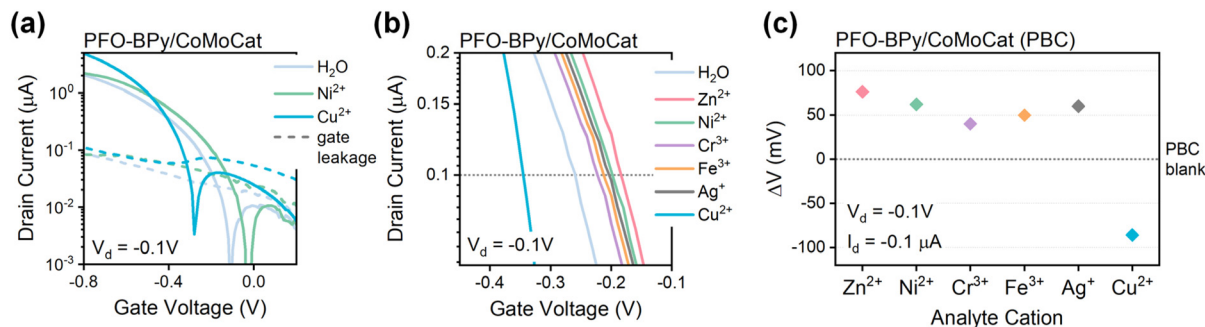
**Fig. 2** (a) Transfer characteristics of PFO-BPy/CoMoCat (PBC) network transistor measured with pure DI water, 15 μM $Ni^{2+}$, and 15 μM $Cu^{2+}$ aqueous solutions as the electrolyte. (b) Zoomed view of the transfer curves for aqueous solutions of all tested metal cations showing the shift to more negative gate voltages only in the presence of $Cu^{2+}$ ions. (c) Voltage shift ($\Delta V$) as sensor response to various metal ions at a fixed drain current of −0.1 μA (dashed line in (b)) with respect to PBC blank sample.

overall on-current. In contrast to that, the presence of $Ni^{2+}$ ions seems to have the opposite – albeit weaker – effect on the turn-on voltage with no significant impact on the on-current. The full range of tested cations is presented in Fig. 2b. Compared to the reference measurement with DI water, all investigated metal cations tend to shift the corresponding transfer curves toward slightly more positive gate voltages, except for $Cu^{2+}$.

The response of the water-gated PFO-BPy/CoMoCat transistor towards various cation analytes was extracted as the gate voltage shift ($\Delta V$) with respect to the blank measurement (PBC blank) at a constant drain current of −0.1 μA and an applied drain voltage of −0.1 V. Note, that we estimate a standard deviation of about 15–20 mV for the extracted voltage shifts based on the variation of the blank samples between measurements. These shifts are plotted in Fig. 2c. Evidently, all devices show a similar response (positive 50–70 mV shift) toward $Zn^{2+}$, $Ni^{2+}$, $Cr^{3+}$, $Fe^{3+}$ and $Ag^+$ ions, whereas the response differs substantially in the presence of $Cu^{2+}$ ions with a voltage shift of approximately −100 mV. This negative voltage shift indicates a clear molecular interaction of cupric ions with the PFO-BPy/CoMoCat network beyond simple variation of ionic strength of the electrolyte and hence Debye layer thickness. Based on previous reports on structurally similar molecules,[40–42] as well as molecular bipyridine and 1,10-phenanthroline[43] we presume that the $Cu^{2+}$ ions interact strongly with the nitrogen of the bipyridine unit to form a stable complex. The binding configuration might be similar to that of the previously reported complex of $Re(CO)_5Cl$ with PFO-BPy.[37,38] However, unwrapping of the polymer from the SWNTs is unlikely to occur due the insolubility of PFO-BPy in water.

To confirm the selective interaction of $Cu^{2+}$ ions with the bipyridine units of the wrapping polymer PFO-BPy, a reference transistor was prepared with a drop-cast network of CoMoCat SWNTs dispersed with PFO as the wrapping polymer (see Fig. 1a), which does not contain any moieties that could form metal complexes. The same conditioning steps (see ESI, Fig. S3†) were applied prior to the acquisition of the transfer curves. These confirmed again that an equilibrium was reached after the first couple of cycles. However, compared to

the transfer characteristics of PFO-BPy/CoMoCat network transistors, the hole currents were higher (probably because of slight variations of the network density) and the turn-on voltage was substantially more positive. Such p-doping of nanotubes in the presence of oxygen and water is expected[44] but was not observed for PFO-BPy-wrapped nanotubes. This difference can be explained by the electron-donating lone-pair electrons of the nitrogen atoms in the bipyridine units of PFO-BPy, which slightly n-dope the semiconducting SWNTs as shown recently by Li *et al.*[27] and thus counteract the usual p-doping of nanotubes in air/water.[45]

In contrast to the strong response toward $Cu^{2+}$ by the water-gated transistors with PFO-BPy/CoMoCat networks, the nearly identical PFO/CoMoCat network transistors do not show any sensitivity toward $Cu^{2+}$ or any other tested metal cation. Fig. 3a shows the transfer characteristics (only forward sweeps) of the latter devices measured under the same conditions using DI water, and aqueous solutions of 15 μM $Ni^{2+}$ and 15 μM $Cu^{2+}$. Regardless of the employed analyte, the transfer curves only show a small turn-on voltage shift to more positive values as also summarized in Fig. 3b and c for all other tested metal cations. The turn-on voltage shift with respect to the blank (PC blank) at constant drain voltage of −0.1 V and drain current of −0.1 μA stayed below 30 mV for all tested analytes and without any particular selectivity for any of them. The overall weaker shifts for all metal salt solutions compared to the PFO-BPy/CoMoCat devices may also be rationalized with the slightly smaller bandgap of (7,5) nanotubes (1.21 eV) compared to (6,5) SWNTs (1.27 eV).

Clearly, the presence of the bipyridine units is crucial for the observed negative gate voltage shift and selectivity towards $Cu^{2+}$ ions by the PFO-BPy/CoMoCat network devices. Overall, we can rule out any generalized interaction of $Cu^{2+}$ with semiconducting nanotubes, further corroborating the assumed complexation with the bipyridine unit. The presence of positively charged copper ions within the Debye length of the electric double layer around the nanotubes should result in additional n-doping (or compensation of p-doping) of the nanotubes and hence a shift of the turn-on voltage to more
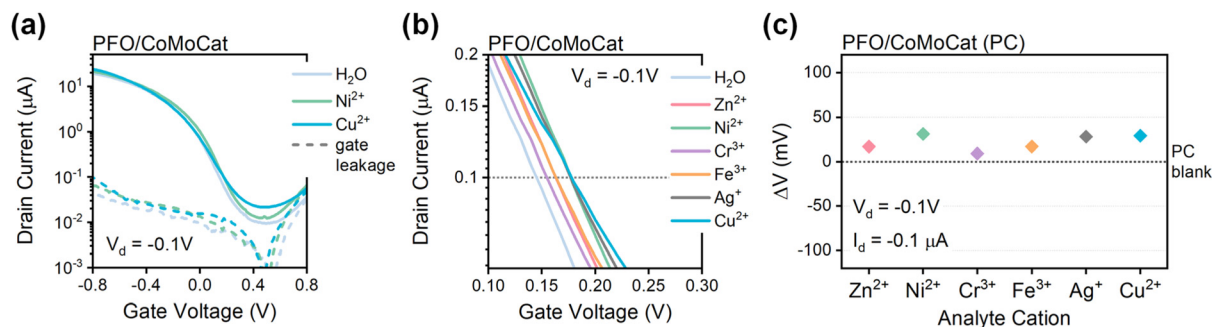
Fig. 3 (a) Transfer characteristics of a reference PFO/CoMoCat (PC) network transistor recorded with pure DI water, 15 μM Ni²⁺, and 15 μM Cu²⁺ solutions as the electrolyte. (b) Zoomed view of the transfer curves showing similar shifts for all metal ions. (c) Voltage shift (ΔV) as sensor response to various metal ions at a fixed drain current of −0.1 μA *versus* PC blank.

negative values. The opposite shift induced by the other cations might be explained by changes of the overall ionic strength of the electrolyte (including the nitrate anions) and thus the capacitance of the electric double layer.[39,46] However, no systematic shift based on the expected total ion concentration was observed.

The impact of the Cu²⁺ concentration on the voltage shift of PFO-BPy/CoMoCat network transistors was investigated for a wide range of concentrations between 3 nM to 150 μM *versus* a blank measurement (PBC blank). Fig. 4a shows selected transfer characteristics (forward sweeps) corresponding to different concentrations of Cu²⁺ ions. As the concentration increases, the transfer curves shift substantially toward more negative voltages. The full range of concentrations is displayed in Fig. 4b, from which the voltage shifts at a fixed drain current (−0.1 μA) depending on the Cu²⁺ ion concentration were extracted and are summarized in Fig. 4c. The voltage shift of ΔV = −22 mV at a Cu²⁺ concentration of 0.1 μM increased to −116 mV for a concentration of 15 μM, reaching −200 mV for 150 μM. The logarithmic plot of ΔV *versus* the concentration does not give a clear linear dependence as might be expected. At very low concentrations the voltage shifts are still within the uncertainty limits and the plot remains relatively flat. However, for higher concentrations (>3 μM) a slope of about 100 mV per decade can be extracted, which is within the expected range for binding and detection of a doubly charged cation. Based on

the uncertainty of the voltage shifts for these devices (see above) we may estimate the limit of detection for Cu²⁺ ions to be around 100 nM.

In summary, a simple dropcast network of PFO-BPy-wrapped CoMoCat SWNTs can be used to selectively and quantitatively detect micromolar levels of Cu²⁺ ions with a good detection range. Next, the response of the Cu²⁺/PFO-BPy/CoMoCat complex toward the still ubiquitous but harmful herbicide glyphosate[47] in water was studied. Competitive binding of Cu²⁺ by glyphosate[48] has been widely used as a detection scheme[42,47,49,50] and should lead to a backshift of the transfer curves of PFO-BPy/CoMoCat transistors treated with Cu²⁺.

To test this sensing concept, a PFO-BPy/CoMoCat SWNT network was exposed to an aqueous solution of 300 μM Cu²⁺ and conditioned with 10 consecutive transfer curve cycles (sweep rate ~50 mV s⁻¹, total measurement time ~13 min) to saturate all exposed bipyridine units with cupric ions and thus reach a reproducible starting point. After removing the Cu²⁺ solution and rinsing the nanotube network with DI water, a blank measurement (PBC-Cu blank) was performed with pure water. The blank measurement showed a large and stable negative turn-on voltage as expected due to the binding of the copper(ii) ions. Subsequently, aqueous solutions with different concentrations of glyphosate were introduced. The corresponding transfer curves (forward sweeps) are shown in Fig. 5a. A substantial backshift of the turn-on voltages to more positive
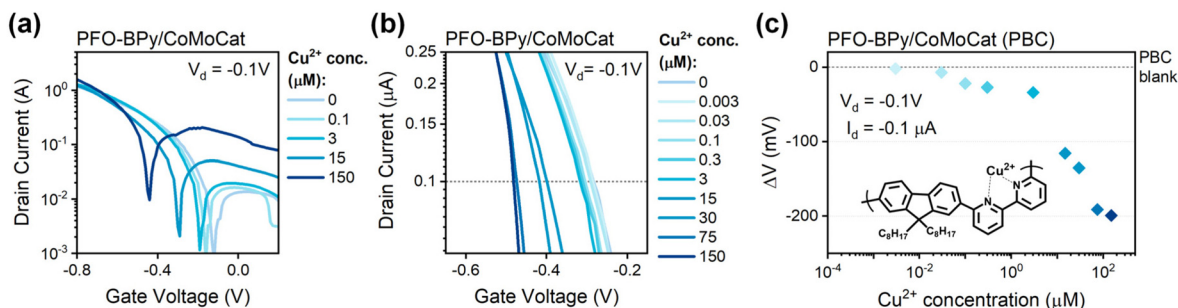


Fig. 4 (a) Transfer characteristics of PFO-BPy/CoMoCat network transistors recorded for a large range of Cu²⁺ concentrations. (b) Zoomed view of the transfer characteristics showing shifts to more negative gate voltages with increasing Cu²⁺ concentration. (c) Correlation of voltage shift (ΔV) with increasing Cu²⁺ concentration at a fixed drain current of −0.1 μA. Inset: possible interaction of Cu²⁺ with bipyridine unit of PFO-BPy.
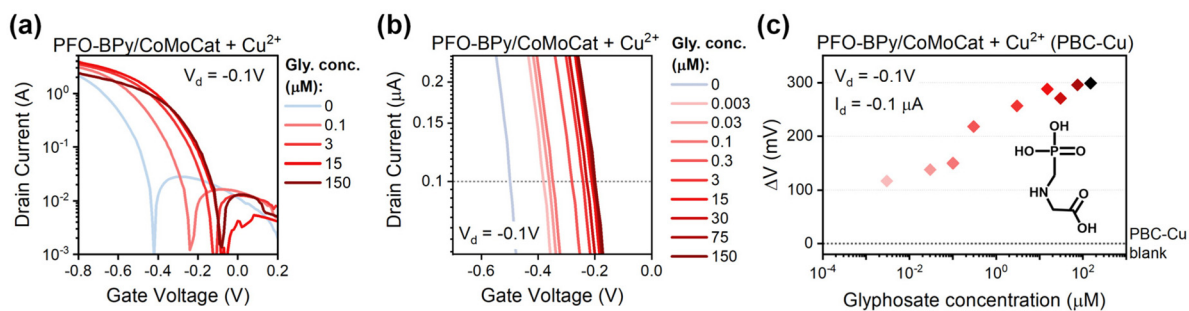
**Fig. 5** (a) Transfer characteristics of $Cu^{2+}$-treated PFO-BPy/CoMoCat (PBC-Cu) network transistors measured for a range of glyphosate (Gly) concentrations. (b) Zoomed view of the transfer curves showing shift to more positive gate voltages with increasing glyphosate concentration. (c) Correlation of the voltage shift ($\Delta V$) with glyphosate concentration at a fixed drain current of $-0.1$ µA *versus* PBC-Cu blank. Inset: molecular structure of glyphosate.

values with increasing glyphosate concentration is evident. The response to a wider range of glyphosate concentrations and a zoomed-in view of the forward sweeps are shown in Fig. 5b. The data clearly indicate the reversal of the initial shift caused by the cupric ions as they are bound by the herbicide. Fig. 5c summarizes the extracted voltage shifts ($\Delta V$) at constant drain voltage ($-0.1$ V) and drain current ($-0.1$ µA) *versus* the glyphosate concentration.

The demonstrated $Cu^{2+}$/PFO-BPy/CoMoCat SWNT network transistor exhibits excellent sensitivity toward glyphosate with large shifts. Even nanomolar concentrations of the herbicide can be detected with a possible limit of detection of 1 nM. The already substantial voltage shift of $+117$ mV at a glyphosate concentration of only 3 nM increases to up to $+288$ mV for 15 µM and can reach up to 300 mV at 150 µM of glyphosate. The detection range is thus within typical and useful limits of glyphosate contamination in water.[47] The slope of the logarithmic plot is about 44 mV per decade (approximately half of that for $Cu^{2+}$, see above), indicating that two glyphosate molecules are required to form a complex[48] and remove or neutralize one $Cu^{2+}$ ion from the PFO-BPy-wrapped nanotubes. Note that PFO-BPy/CoMoCat SWNT networks could be re-used for several glyphosate measurements but re-saturation of the exposed bipyridine units with cupric ions was necessary.

Similar to glyphosate, pyrophosphates (PPi) can also bind cupric ions. Abnormalities of pyrophosphate levels in the human body can be responsible for or indicators of various diseases.[51,52] Hence, their quantitative detection (usually using fluorescence probes) has been investigated for some time.[53–57] In analogy to glyphosate, we also employed the $Cu^{2+}$-treated PFO-BPy/CoMoCat transistors to detect pyrophosphate anions in water as shown in Fig. S4 (ESI†). Nanomolar levels of pyrophosphate resulted in measurable voltage shifts. Overall a wide range of concentrations from a few tens of nM to 100 µM correlated directly with positive voltage shifts between $+150$ and $+300$ mV (slope ~45 mV per decade).

So far, we have only shown transistor responses for analytes in DI water, which clearly is not a typical sample due to the low ionic strength. Hence, we also tested the responsivity of our devices to glyphosate in regular tap water. For this measurement, the $Cu^{2+}$-treated PFO-BPy/CoMoCat SWNT network was formed as described above and a blank measurement was acquired with tap water (PBC-Cu blank). Five different concentrations of glyphosate were added to the tap water samples. The corresponding transfer characteristics are shown in Fig. 6a. The extracted voltage shifts of the forward sweeps (see Fig. 6b and c) were smaller compared to the DI water samples and the corresponding slope was lower (only
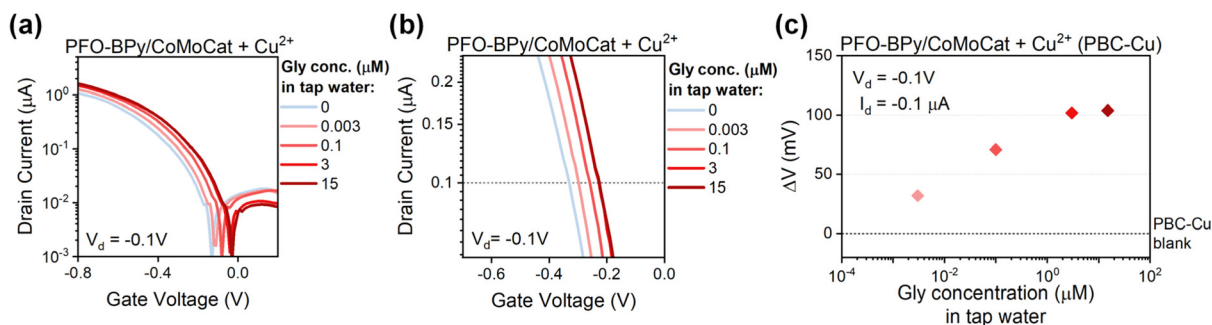


**Fig. 6** (a) Transfer characteristics of $Cu^{2+}$-treated PFO-BPy/CoMoCat (PBC-Cu) network transistors recorded for a range of glyphosate (Gly) concentrations in regular tap water. (b) Zoomed view of transfer curves showing a shift to more positive gate voltages with increasing glyphosate concentration. (c) Correlation of voltage shift ($\Delta V$) with glyphosate concentration in tap water at a fixed drain current of $-0.1$ µA *versus* PBC-Cu blank.

~20 mV per decade). Nevertheless, the overall trend remained the same and should enable reliable glyphosate detection in regular water after suitable calibration.

## Conclusions

In summary we have demonstrated the highly selective response of water-gated transistors with PFO-BPy-wrapped (6,5) SWNT networks to $Cu^{2+}$ ions mediated by complexation with the bipyridine units of the polymer. The presence of the positively charged cupric ions in close proximity to the SWNTs counteracts hole accumulation and thus leads to a shift of the transfer curves to more negative gate voltages. The voltage shift can be used for the quantification of $Cu^{2+}$ ion concentration between 0.1 μM and 100 μM. No additional functionalization of the nanotubes was required. This observation also highlights the need for proper referencing when using polymer-wrapped nanotubes in sensors. Unexpected and unwanted interactions with the wrapping polymer may interfere with the desired sensor function, possibly leading to erroneous measurements. As shown here, polyfluorenes such as PFO without additional functional moieties could be employed in that case.

Furthermore, the $Cu^{2+}$–bipyridine complex on the PFO-BPy wrapped SWNTs can be used as a secondary probe for the detection and quantification of the herbicide glyphosate in water at nanomolar levels as well as biologically important pyrophosphates. Relevant concentrations of glyphosate could even be detected when using regular tap water as the electrolyte, demonstrating the applicability of this sensor concept for real-world samples in an environmental/agricultural context.

## Experimental details

### Materials

CoMoCat nanotube raw material (SG65i, Sigma Aldrich, average diameter 0.78 nm) and wrapping polymers poly[(9,9-dioctylfluorenyl-2,7-diyl)-*alt*-(6,6′-[2,2′-bipyridine])] (PFO-BPy, American Dye Source, $M_w$ = 40 kg mol$^{-1}$) and poly(9,9-dioctylfluorene) (PFO, $M_w$ > 20 kg mol$^{-1}$, Sigma Aldrich) were purchased and used as described below. The analytes glyphosate (certified reference material), sodium pyrophosphate dibasic (≥99.0%), copper(II) nitrate hydrate (99.999%), zinc nitrate hexahydrate (≥99.0%), nickel nitrate hexahydrate (99.999%), chromium(III) nitrate nonahydrate (99%), iron(III) nitrate nonahydrate (≥99.95%) and silver nitrate (99.995%) were purchased from Sigma-Aldrich and used without further purification. Stock solutions of each analyte were prepared in DI water at a concentration of 3 mM. Further dilutions were prepared as mentioned below.

### Preparation of CoMoCat dispersions with PFO-BPy

Direct dispersions of CoMoCat raw material with the conjugated polymer PFO-BPy were prepared as described pre-viously[34] with minor modifications. Prior to the dispersion process, CoMoCat raw material was dried at 130 °C for 1 day to remove moisture as it can cause problems regarding the quality and yield of the resulting dispersion. Dried CoMoCat powder was combined with a solution of PFO-BPy in toluene at the final concentrations of 0.38 g L$^{-1}$ and 0.5 g L$^{-1}$, respectively. The exfoliation process was carried out using a Silverson L2/Air shear force mixer at its maximum speed of 10 230 rpm for 3 days. The dispersion temperature was controlled using a chiller at 20 °C to maximize the yield. In order to separate the non-exfoliated material, the dispersion was centrifuged twice at 60 000$g$ for 45 min (Beckman Coulter Avanti J26XP centrifuge). The resulting supernatant with (6,5) SWNTs was filtered through a syringe filter (Whatman, PTFE, 5 μm pore size) to remove any residues of the non-exfoliated material. Excess free polymer was eliminated by filtration of the dispersion through a polytetrafluoroethylene membrane filter (Merck Omnipore, JVWP, pore size 0.1 μm, diameter 25 mm), and the obtained filter cake was re-dispersed in pure toluene using bath sonication for 30 min and centrifuged at 60 000$g$ for 30 min to remove any bundles.

### Preparation of CoMoCat dispersions with PFO

Dispersions of CoMoCat SWNTs with the conjugated polymer PFO were prepared in a similar manner, with some adjustments. Prior to dispersing, the CoMoCat raw material was dried at 130 °C for 1 day to remove moisture. 100 mg of the CoMoCat material were added to a solution of 225 mg of PFO in 250 mL of toluene. Shear force mixing was conducted with a Silverson L2/Air (10 230 rpm) for 3 days, with the temperature being kept constant at 20 °C. The same post-exfoliation procedure was followed including the two-step centrifugation at 60 000$g$ for 45 min, syringe filtration (Whatman, PTFE, 5 μm pore size), and vacuum filtration through a polytetrafluoroethylene membrane filter (Merck Omnipore, JVWP, pore size 0.1 μm, diameter 25 mm). The obtained filter cake was re-dispersed in pure toluene using bath sonication for 30 min and centrifuged at 60 000$g$ for 30 min to remove any bundles.

### Characterization of dispersions

Absorbance spectra of all dispersions were acquired using a Cary 6000i spectrometer (Varian Inc.) and a cuvette with 1 cm optical path length.

A Fluorolog 3 spectrometer (Horiba Jobin–Yvon GmbH) equipped with a xenon lamp (450 W) with a double monochromator for excitation and a cooled InGaAs diode array (800–1600 nm) for detection was employed to collect photoluminescence excitation emission (PLE) maps for the polymer/SWNT hybrid dispersions. The measurements were conducted under ambient conditions using a 4 × 10 mm quartz cuvette. The emission intensities in all maps were normalized to the power of the excitation light source at the corresponding wavelength and further corrected using the wavelength-dependent sensitivity of the detector.

## Device fabrication

Interdigitated source–drain electrodes with a channel length of 20 μm and channel width of 10 mm, as well as a side gate electrode were patterned by standard double layer resist (MicroChem LOR5B/Mic256posit S1813) photolithography on glass substrates (SCHOTT AG, AF32 Eco). Chromium (2 nm) and gold (30 nm) were deposited consecutively using electron-beam evaporation and a subsequent lift-off was performed in *N*-methyl-2-pyrrolidone. Prior to SWNT deposition, the substrates were cleaned by bath sonication in acetone and 2-propanol, followed by UV-ozone cleaning (UV Ozone Cleaner, Ossila Ltd). The prepared dispersions of CoMoCat SWNTs were dropcast (25 μL) onto the interdigitated electrode area while heating the substrates to 80 °C.

## Device measurements

Transfer characteristics of the water-gated field-effect transistors were acquired using a semiconductor parameter analyzer (Agilent 4155C) under ambient conditions. For all measurements, a constant drain voltage ($V_d$) of −0.1 V was applied while the gate voltage ($V_g$) was swept from 0.8 V to −0.8 V. A custom-made polytetra-fluoroethylene (PTFE) substrate holder with a reservoir covering the entire interdigitated electrode area and the gate electrode was employed. Aqueous solutions of the analytes were prepared as described below and filled into the PTFE reservoir as the electrolyte. All devices were conditioned with the corresponding analyte by performing 10 consecutive cycles (sweep rate ~50 mV s$^{-1}$, total measurement time ~13 min) before the acquisition of the presented transfer curves to ensure that no further shifts occurred.

To study the impact of different metal ions, a blank measurement was obtained with DI water before introducing any metal ion solution and used as the reference. Aqueous solutions of $Zn^{2+}$, $Ni^{2+}$, $Cr^{3+}$, $Fe^{3+}$, $Ag^+$ and $Cu^{2+}$ were used at a fixed concentration of 15 μM in the given order and repeated blank measurements were conducted using DI water between two metal ion solutions. Note that due to the valency of the cations the corresponding nitrate concentration was 15, 30 or 45 μM and the ionic strength varied from 15 μM (for $AgNO_3$), 45 μM (for $Cu(NO_3)_2$, $Zn(NO_3)_2$, $Ni(NO_3)_2$) to 90 μM (for $Fe(NO_3)_3$, $Cr(NO_3)_3$).

For experiments with different $Cu^{2+}$ concentrations, a blank measurement was recorded using DI water before introducing the $Cu^{2+}$ solutions and used as the reference. Aqueous solutions of $Cu^{2+}$ were prepared at concentrations of 0.003 μM, 0.03 μM, 0.1 μM, 0.3 μM, 3 μM, 15 μM, 30 μM, 75 μM and 150 μM. Starting from the lowest concentration, the measurements were conducted without blank measurements between the $Cu^{2+}$ solutions.

For the detection of various glyphosate (Gly) concentrations, the nanotube networks were exposed to 300 μM $Cu^{2+}$ solution and conditioned for 10 consecutive cycles to saturate the bipyridine units with $Cu^{2+}$ ions. Next, a blank measurement was performed with DI water before introducing the glyphosate solutions and used as the reference. Aqueous solu-

tions of glyphosate were prepared at concentrations of 0.003 μM, 0.03 μM, 0.1 μM, 0.3 μM, 3 μM, 15 μM, 30 μM, 75 μM and 150 μM. Starting from the lowest concentration, all measurements were recorded without blank measurements between the different glyphosate solutions.

The impact of pyrophosphate (PPi) was studied following the same procedure as for glyphosate, using a $Cu^{2+}$ saturated nanotube network with the same concentrations as above.

For the detection of glyphosate in regular tap water, the devices were saturated with $Cu^{2+}$ ions using a 300 μM $Cu^{2+}$ solution and conditioned with 10 consecutive cycles. Next, the reservoir was filled with tap water (as obtained without further purification, Heidelberg-Neuenheim, Germany) and transfer curves were recorded as blank reference. Solutions of glyphosate were prepared at concentrations of 0.003 μM, 0.1 μM, 3 μM and 15 μM in the same tap water and used in the given order as the analyte. The transistor measurements were conducted without any blanks between the different glyphosate solutions.

## Author contributions

M.B.L. carried out the experiments, analysed the data and wrote the manuscript. S.L. provided PFO-wrapped nanotubes. D.H. designed the setup for device measurements with water. J.Z. conceived and supervised the project and co-wrote the manuscript.

## Conflicts of interest

There are no conflicts to declare.

## Acknowledgements

## References

1  S. G. Bucella, J. M. Salazar-Rios, V. Derenskyi, M. Fritsch, U. Scherf, M. A. Loi and M. Caironi, *Adv. Electron. Mater.*, 2016, **2**, 1600094.

2  B. Kim, M. L. Geier, M. C. Hersam and A. Dodabalapur, *Sci. Rep.*, 2017, **7**, 39627.

3  M. Ha, J.-W. T. Seo, P. L. Prabhumirashi, W. Zhang, M. L. Geier, M. J. Renn, C. H. Kim, M. C. Hersam and C. D. Frisbie, *Nano Lett.*, 2013, **13**, 954–960.

4  C. Cao, J. B. Andrews and A. D. Franklin, *Adv. Electron. Mater.*, 2017, **3**, 1700057.

5  M. Rother, M. Brohmann, S. Yang, S. B. Grimm, S. P. Schießl, A. Graf and J. Zaumseil, *Adv. Electron. Mater.*, 2017, **3**, 1700080.

6  N. X. Williams, G. Bullard, N. Brooke, M. J. Therien and A. D. Franklin, *Nat. Electron.*, 2021, **4**, 261–268.

7  S. Schneider, J. Lefebvre, N. J. Diercks, F. J. Berger, F. Lapointe, J. Schleicher, P. R. L. Malenfant and J. Zaumseil, *ACS Appl. Nano Mater.*, 2020, **3**, 12314–12324.

8  L. Liu, J. Han, L. Xu, J. Zhou, C. Zhao, S. Ding, H. Shi, M. Xiao, L. Ding, Z. Ma, C. Jin, Z. Zhang and L.-M. Peng, *Science*, 2020, **368**, 850–856.

9  F. Yang, M. Wang, D. Zhang, J. Yang, M. Zheng and Y. Li, *Chem. Rev.*, 2020, **120**, 2693–2758.

10 T. Srimani, J. Ding, A. Yu, P. Kanhaiya, C. Lau, R. Ho, J. Humes, C. T. Kingston, P. R. L. Malenfant and M. M. Shulaker, *Adv. Electron. Mater.*, 2022, 2101377.

11 V. Schroeder, S. Savagatrup, M. He, S. Lin and T. M. Swager, *Chem. Rev.*, 2019, **119**, 599–663.

12 B. Shkodra, M. Petrelli, M. A. C. Angeli, D. Garoli, N. Nakatsuka, P. Lugli and L. Petti, *Appl. Phys. Rev.*, 2021, **8**, 041325.

13 A. Molazemhosseini, F. A. Viola, F. J. Berger, N. F. Zorn, J. Zaumseil and M. Caironi, *ACS Appl. Electron. Mater.*, 2021, **3**, 3106–3113.

14 F. Scuratti, G. E. Bonacchini, C. Bossio, J. M. Salazar-Rios, W. Talsma, M. A. Loi, M. R. Antognazza and M. Caironi, *ACS Appl. Mater. Interfaces*, 2019, **11**, 37966–37972.

15 S. Ishihara, C. J. O'Kelly, T. Tanaka, H. Kataura, J. Labuta, Y. Shingaya, T. Nakayama, T. Ohsawa, T. Nakanishi and T. M. Swager, *ACS Appl. Mater. Interfaces*, 2017, **9**, 38062–38067.

16 Z. Yaari, Y. Yang, E. Apfelbaum, C. Cupo, A. H. Settle, Q. Cullen, W. Cai, K. L. Roche, D. A. Levine, M. Fleisher, L. Ramanathan, M. Zheng, A. Jagota and D. A. Heller, *Sci. Adv.*, 2021, **7**, eabj0852.

17 J. D. Harvey, H. A. Baker, M. V. Ortiz, A. Kentsis and D. A. Heller, *ACS Sens.*, 2019, **4**, 1236–1244.

18 M. S. Filipiak, M. Rother, N. M. Andoy, A. C. Knudsen, S. Grimm, C. Bachran, L. K. Swee, J. Zaumseil and A. Tarasov, *Sens. Actuators, B*, 2018, **255**, 1507–1516.

19 M. Berto, M. Di Giosia, M. Giordani, M. Sensi, F. Valle, A. Alessandrini, C. Menozzi, A. Cantelli, G. C. Gazzadi, F. Zerbetto, M. Calvaresi, F. Biscarini and C. A. Bortolotti, *Adv. Electron. Mater.*, 2021, **7**, 2001114.

20 M. Balcı Leinen, P. Klein, F. L. Sebastian, N. F. Zorn, S. Adamczyk, S. Allard, U. Scherf and J. Zaumseil, *Adv. Electron. Mater.*, 2020, **6**, 2000717.

21 C. Guo, J. Ouyang, H. Shin, J. Ding, Z. Li, F. Lapointe, J. Lefebvre, A. J. Kell and P. R. L. Malenfant, *ACS Sens.*, 2020, **5**, 2136–2145.

22 S. G. Song, S. Ha, H. J. Cho, M. Lee, D. Jung, J.-H. Han and C. Song, *ACS Appl. Nano Mater.*, 2019, **2**, 109–117.

23 D. Fong, J. Yeung, E. Meichsner and A. Adronov, *ACS Appl. Polym. Mater.*, 2019, **1**, 797–803.

24 M. Bariya, H. Y. Y. Nyein and A. Javey, *Nat. Electron.*, 2018, **1**, 160–171.

25 S.-C. Park, H. J. Jeong, M. Heo, J. H. Shin and J.-H. Ahn, *ACS Appl. Electron. Mater.*, 2021, **3**, 2580–2588.

26 K. Melzer, V. D. Bhatt, T. Schuster, E. Jaworska, K. Maksymiuk, A. Michalska, P. Lugli and G. Scarpa, *IEEE Sens. J.*, 2015, **15**, 3127–3134.

27 Z. Li, J. Ding, J. Ouyang and P. R. L. Malenfant, *ACS Appl. Electron. Mater.*, 2021, **3**, 4424–4432.

28 N. A. Rice, W. J. Bodnaryk, B. Mirka, O. A. Melville, A. Adronov and B. H. Lessard, *Adv. Electron. Mater.*, 2019, **5**, 1800539.

29 S. G. Bucella, J. M. Salazar-Rios, V. Derenskyi, M. Fritsch, U. Scherf, M. A. Loi and M. Caironi, *Adv. Electron. Mater.*, 2016, **2**, 1600094.

30 D. Heimfarth, M. Balcı Leinen, P. Klein, S. Allard, U. Scherf and J. Zaumseil, *ACS Appl. Mater. Interfaces*, 2022, **14**, 8209–8217.

31 A. Nish, J. Y. Hwang, J. Doig and R. J. Nicholas, *Nat. Nanotechnol.*, 2007, **2**, 640–646.

32 F. A. Lemasson, T. Strunk, P. Gerstel, F. Hennrich, S. Lebedkin, C. Barner-Kowollik, W. Wenzel, M. M. Kappes and M. Mayor, *J. Am. Chem. Soc.*, 2011, **133**, 652–655.

33 H. Ozawa, N. Ide, T. Fujigaya, Y. Niidome and N. Nakashima, *Chem. Lett.*, 2011, **40**, 239–241.

34 A. Graf, Y. Zakharko, S. P. Schießl, C. Backes, M. Pfohl, B. S. Flavel and J. Zaumseil, *Carbon*, 2016, **105**, 593–599.

35 K. R. Jinkins, S. M. Foradori, V. Saraswat, R. M. Jacobberger, J. H. Dwyer, P. Gopalan, A. Berson and M. S. Arnold, *Sci. Adv.*, 2021, **7**, eabh0640.

36 R. B. Weisman and S. M. Bachilo, *Nano Lett.*, 2003, **3**, 1235–1238.

37 Y. Joo, G. J. Brady, M. J. Shea, M. B. Oviedo, C. Kanimozhi, S. K. Schmitt, B. M. Wong, M. S. Arnold and P. Gopalan, *ACS Nano*, 2015, **9**, 10203–10213.

38 M. Brohmann, M. Rother, S. P. Schiessl, E. Preis, S. Allard, U. Scherf and J. Zaumseil, *J. Phys. Chem. C*, 2018, **122**, 19886–19896.

39 T. Cramer, A. Campana, F. Leonardi, S. Casalini, A. Kyndiah, M. Murgia and F. Biscarini, *J. Mater. Chem. B*, 2013, **1**, 3728–3741.

40 R. Mitobe, Y. Sasaki, W. Tang, Q. Zhou, X. Lyu, K. Ohshiro, M. Kamiko and T. Minami, *ACS Appl. Mater. Interfaces*, 2022, **14**, 22903–22911.

41 P. Gayathri and A. Senthil Kumar, *Langmuir*, 2014, **30**, 10513–10521.

42 M. Gui, J. Jiang, X. Wang, Y. Yan, S. Li, X. Xiao, T. Liu, T. Liu and Y. Feng, *Sens. Actuators, B*, 2017, **243**, 696–703.

43 G. Anderegg, *Helv. Chim. Acta*, 1963, **46**, 2397–2410.

44 C. M. Aguirre, P. L. Levesque, M. Paillet, F. Lapointe, B. C. St-Antoine, P. Desjardins and R. Martel, *Adv. Mater.*, 2009, **21**, 3087–3091.

45 M. B. Leinen, F. J. Berger, P. Klein, M. Mühlinghaus, N. F. Zorn, S. Settele, S. Allard, U. Scherf and J. Zaumseil, *J. Phys. Chem. C*, 2019, **123**, 2280–22689.

46 J. Li, P. H. Q. Pham, W. Zhou, T. D. Pham and P. J. Burke, *ACS Nano*, 2018, **12**, 9763–9774.

47 A. L. Valle, F. C. C. Mello, R. P. Alves-Balvedi, L. P. Rodrigues and L. R. Goulart, *Environ. Chem. Lett.*, 2019, **17**, 291–317.

48 J. Sheals, P. Persson and B. Hedman, *Inorg. Chem.*, 2001, **40**, 4302–4309.

49 K. Asano, P. Didier, K. Ohshiro, N. Lobato-Dauzier, A. J. Genot, T. Minamiki, T. Fujii and T. Minami, *Langmuir*, 2021, **37**, 7305–7311.

50 Y. Sasaki, K. Asano, T. Minamiki, Z. Zhang, S.-y. Takizawa, R. Kubota and T. Minami, *Chem. – Eur. J.*, 2020, **26**, 14525–14529.

51 M. Doherty, C. Belcher, M. Regan, A. Jones and J. Ledingham, *Ann. Rheum. Dis.*, 1996, **55**, 432–436.

52 A. E. Timms, Y. Zhang, R. G. G. Russell and M. A. Brown, *Rheumatology*, 2002, **41**, 725–729.

53 Y. Bao, H. Wang, Q. Li, B. Liu, Q. Li, W. Bai, B. Jin and R. Bai, *Macromolecules*, 2012, **45**, 3394–3401.

54 J. Yang, R. Acharya, X. Zhu, M. E. Köse and K. S. Schanze, *ACS Omega*, 2016, **1**, 648–655.

55 M. Guan, C. Xu, J. Ma, T. Yang, J. Liu and G. Feng, *Anal. Sci.*, 2019, **35**, 625–630.

56 S. Dey and P. K. Sukul, *ACS Omega*, 2019, **4**, 16191–16200.

57 S. K. Kim, D. H. Lee, J.-I. Hong and J. Yoon, *Acc. Chem. Res.*, 2009, **42**, 23–31.